Alignment of Lamellar Block Copolymer Microstructure in an Electric Field. 2. Mechanisms of Alignment

Karl Amundson,* Eugene Helfand, Xina Quan, and Steven D. Hudson

AT&T Bell Laboratories, Murray Hill, New Jersey 07974

Steven D. Smith

The Procter and Gamble Company, Cincinnati, Ohio 45239

Received May 5, 1994; Revised Manuscript Received August 12, 1994[⊗]

ABSTRACT: Alignment of lamellar block copolymer microstructure in an electric field was studied. Two mechanisms of alignment are considered: selective electric-field-induced disordering and alignment through movement of defects. The latter mechanism is supported by the findings that, in an aligned sample, defect structures exhibited a highly anisotropic arrangement and were spatially clumped. An analysis of field-induced forces on disclination lines and defect walls is presented. Also, defect interactions are considered. Through the interplay between these forces, the alignment process, the kinetics of alignment, and clumping of defects can be rationalized.

I. Introduction

Alignment of block copolymer microstructure by deformation or flow has been studied extensively.[1-8] Recently, we have reported on the alignment of lamellar block copolymer microstructure in the relatively weak aligning force induced by an electric field.[9,10] The most recent paper[10] focused primarily upon alignment kinetics. Here, we report on the morphology of the microstructure in aligned block copolymers and what it indicates about the mechanisms of alignment.

The driving force for alignment is the anisotropic free energy of a block copolymer with a lamellar microstructure. In an electric field, the electrostatic contribution to the free energy density of a block copolymer with lamellar morphology can be expressed to lowest order as[10]

$$\frac{\mathcal{F}-\mathcal{F}_0}{\mathcal{V}} = \frac{1}{8\pi}\epsilon_D|\mathbf{E}_0|^2\left[\left(\frac{\beta}{\epsilon_D}\right)^2\langle\bar{\psi}^2\rangle(\hat{\mathbf{e}}_q\cdot\hat{\mathbf{e}}_z)^2 - \frac{\langle\epsilon\rangle}{\epsilon_D}\right] \quad (1.1)$$

$\mathcal{F}$ is the free energy, $\mathcal{F}_0$ is the free energy in the absence of an electric field, and $\mathcal{V}$ is the volume. ϵ_D is the dielectric constant in the limit of vanishing stationary composition pattern, β is the sensitivity of the dielectric constant to composition, $\beta = d\epsilon/d\psi$, and $\langle\epsilon\rangle$ is a space-average dielectric constant (defined more precisely in ref 10). $\bar{\psi}(\mathbf{r})$ is the compositional order parameter associated with the stationary composition pattern, and $\hat{\mathbf{e}}_q$ is the unit wave vector of the lamellae. $\hat{\mathbf{e}}_z$ is the unit vector in the direction of the applied field, $\mathbf{E}_0$. This expression results from a perturbation expansion in the composition pattern[10] and is strictly valid only when the quantity

$$\frac{\beta^2}{\epsilon_D}\langle\bar{\psi}^2\rangle \quad (1.2)$$

is small. The first term on the right of eq 1 is anisotropic. The microstructural orientation with lowest free energy is such that the Fourier components of the composition pattern have wave vectors (in the direction $\hat{\mathbf{e}}_q$) orthogonal to the applied field. In this paper, the mechanisms by which anisotropic free energy gives rise to aligned microstructure are explored. Clues about the alignment mechanism are drawn from microscopic examination of the defect structures in an aligned block copolymer sample.

II. Experimental Section

Polystyrene–poly(methyl methacrylate) diblock copolymer (PS–PMMA) samples were synthesized anionically. The polymer in this study has a molecular weight average of 37 000 (polydispersity index 1.08) and is 53 vol % polystyrene, as determined by ^{1}H NMR with consideration to density. The order–disorder transition (ODT) was determined rheologically and optically to be in the range 251–256 °C.[11]

The sample cell was described in a previous paper.[10] It is heated by flowing hot nitrogen and allows for simultaneous application of an electric field and birefringence measurement, although birefringence measurements were not used in the study discussed in this paper. The PS–PMMA block copolymer sample was heated to 247 °C (several degrees below the order–disorder transition), at which point an 18 kV/cm electric field was applied. The sample was held at that temperature for approximately 10 min, then cooled 3–4 °C/min to room temperature. The field was applied until the sample cooled to below the glass transition. The small angle X-ray scattering pattern of the sample after alignment is shown in Figure 1. The X-ray beam direction was orthogonal to the direction the electric field was previously applied. The SAXS pattern reveals strong alignment of lamellae in the lowest-energy orientation, where their normal vectors are orthogonal to the electric-field direction.

Microtome slices were taken from the aligned sample (far from any surfaces), stained with ruthenium tetraoxide, and viewed with a transmission electron microscope. The two orientations of slice planes with respect to the direction of electric-field application are shown in Figure 2. Some slice planes were perpendicular to the electric field and are referred to as "perpendicular slices". Other slice planes contained the electric field direction and are referred to as "parallel slices".

III. Morphology of the Aligned Sample

Figure 3 shows portions of typical transmission electron micrographs of "parallel" and "perpendicular" slices. The two types are quite distinct. For perpendicular slices, the dark and light stripes are usually of fairly uniform period. Also, the periodicity of the stripes is usually in approximate agreement with the 23 nm periodicity of the lamellae, as determined by SAXS. This is consistent with the nearly orthogonal intersection of the slice plane with the lamellae, as expected for a field-aligned sample. The orientation of

[⊗] Abstract published in *Advance ACS Abstracts*, September 15, 1994.

0024-9297/94/2227-6559$04.50/0

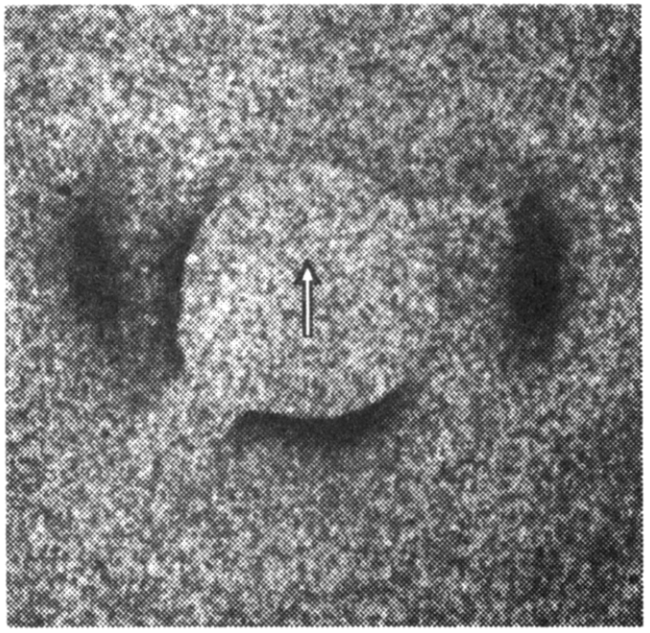

Figure 1. Small angle X-ray scattering pattern from the block copolymer sample after alignment in the electric field. The X-ray beam was orthogonal to the applied field direction which is indicated by the arrow. The two peaks arise from scattering off the lamellar microstructure. Thin arcs near the beamstop result from beam leakage and imperfect beam alignment.

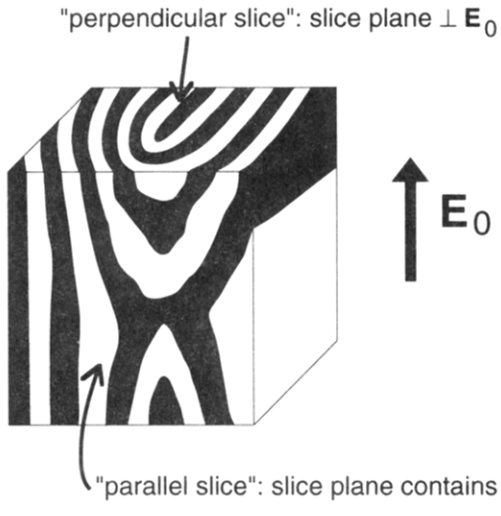

Figure 2. Orientation of slice planes with respect to the direction of the applied field.

the lamellae meanders in the slice plane, however. This is also expected, since all lamellar orientations for which the normal vector is in the plane perpendicular to the electric field make up a degenerate set of lowest-energy orientations.

In addition, four classes of defect structures are identifiable. $+^1/_2$ disclination lines and defect walls are most prevalent. $-^1/_2$ disclination lines and isolated edge dislocations are also observed, but are rarer. These defect structures in smectic-A systems are discussed in books by de Gennes and Prost[12] and Kleman[13] and in numerous reports.[14-17] Disclination lines are lines of singularity in the $\hat{\mathbf{e}}_q$ field. They are characterized by a $\pm\pi$ rotation of the lamellar wave vector upon counterclockwise travel along a loop that circumscribes a type $\pm^1/_2$ disclination line. The points of intersection of some disclination lines with the slice plane are indicated in Figure 3a. Wall defects are planes across which the microstructural pattern makes a discontinuous jump in orientation. Lines of intersection between wall defects and the slice plane are also indicated in Figure 3a.

Representative micrographs of "parallel" sections are shown in Figures 3b,c. Typical views are of fairly uniform patterns, as in Figure 3b and the lower right and upper left of Figure 3c. Striations are primarily along the direction of the applied field, as expected for a field-aligned sample. The repeat distance of the light and dark bands are commonly larger than the 23 nm periodicity of the lamellae, indicative of nonorthogonal intersection of the slice with lamellae. In distinction to Figure 3a, sharp intersections with disclination lines are not prevalent; instead it appears that the trajectories of disclination lines in the aligned sample are predominantly in the direction of the electric field. Also, "disturbances" such as that running through the center of Figure 3c are common. Typically, these regions are long in the direction of the electric field and have a width on the order of 1 μm. In gross view, they are regions of a very coarse pattern, indicating a very shallow intersection of the slice plane with the lamellae. It is likely that these features arise from a disclination line with a trajectory approximately in the slice plane, but offset from the slice plane, as is illustrated in Figure 2. The coarse pattern is similar to a wood grain pattern.

A more detailed analysis of these features reveals additional complexity; there is a high density of short-range defects in these regions. The strong curvature and sharp jumps in lamellar orientation indicate a high density of line and wall defects. The formation of these regions is likely due to defect interactions and defect pinning, as will be discussed in the next section.

As just stated, in the aligned material, disclination lines rune predominantly in the direction of the applied field. In addition, defect walls are anisotropically arranged in the aligned sample. This is best understood by first defining a rotation axis for a wall defect. A rotation plus a translation is required to map the lamellar pattern on one side of a wall defect to the other. We refer to the axis of rotation as the rotation axis for the wall. If the wall contains its rotation axis, it is a bend wall, and if the axis is perpendicular to the wall, it is of twist character. If the rotation axis is somewhere in between, the wall is of mixed character. In the field-aligned sample, the rotation axes of the wall defects are predominantly aligned along the direction of the applied field, $\hat{\mathbf{e}}_z$. Thus, walls with normals parallel to $\hat{\mathbf{e}}_z$ have primarily twist character, while walls with normals nearly perpendicular to $\hat{\mathbf{e}}_z$ have primarily bend character. Examples of bend walls are indicated in Figure 3a.

IV. Mechanisms of Alignment

In this section, two possible alignment mechanisms are examined. First, the destabilizing effect of the electric field on the microstructure in disfavored orientations will be considered. Next alignment by movement of defect structures will be considered.

A. Alignment by Selective Disordering. An electric field has an anisotropic destabilizing effect on lamellar microstructure (see eq 1.1). It is then conceivable that microstructural alignment is achieved by selective disordering in regions where the lamellae are in "disfavored" orientation. This postulate is quantitatively treated here using the thermodynamic potential of Fredrickson and Helfand.[18] The conclusion is that the effect is far too weak to be operative. However, in stronger but experimentally attainable fields, this mechanism is quite possible.

This analysis will consider only weak segregation, and the ordered phase composition pattern will be described

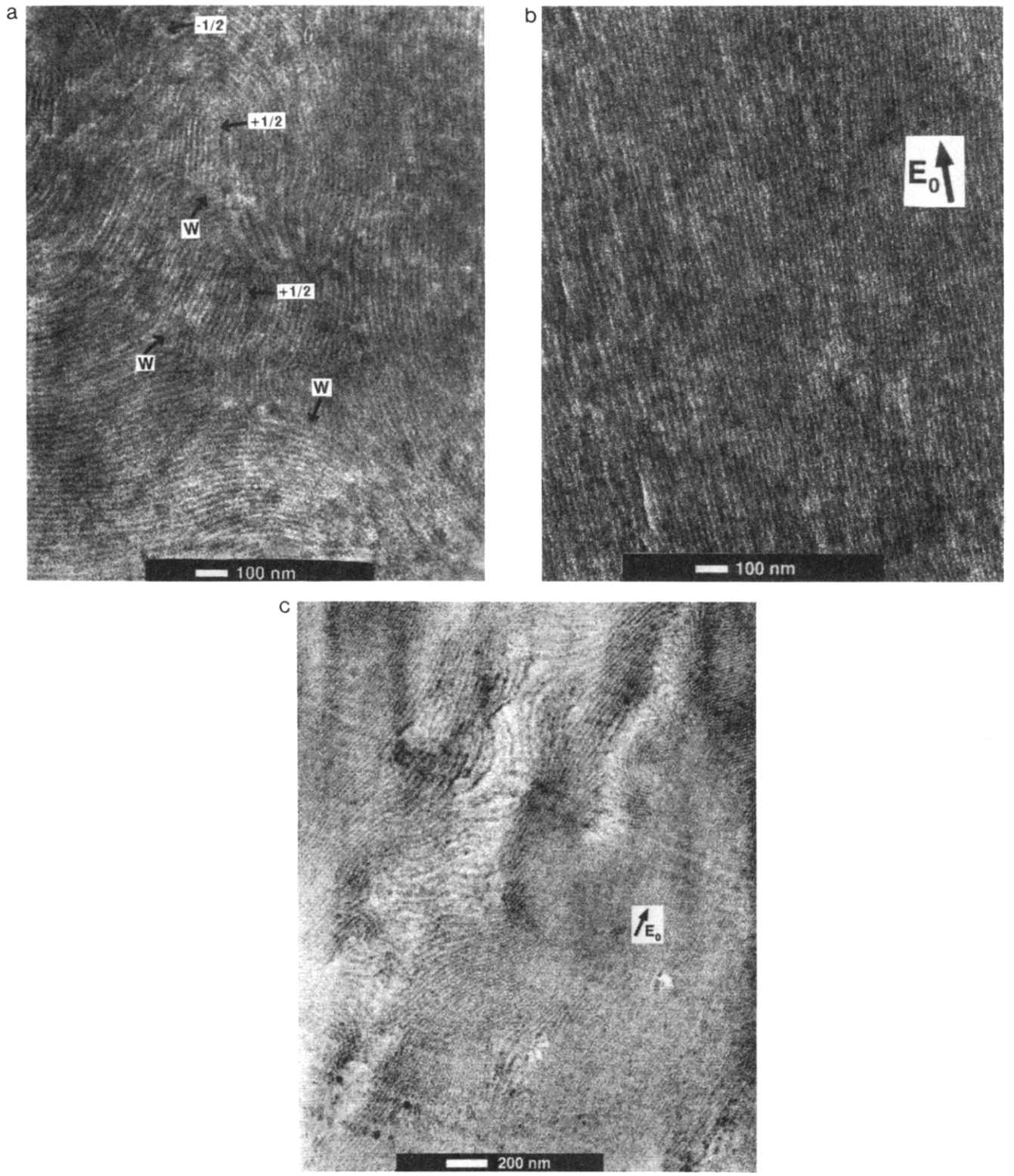

Figure 3. Transmission electron micrographs of microtome slices of an aligned PS–PMMA block copolymer sample. In (a), the slice plane was perpendicular to the electric-field direction, and in (b) and (c) the slice plane contained the electric-field direction. Intersection of the slice plane with $+^1/_2$ and $-^1/_2$ disclination lines and wall defects (denoted with a "w") are indicated in (a).

as sinusoidal:

$$\bar{\psi} = 2A \cos(q^* \mathbf{e}_q \cdot \mathbf{r}) \tag{4.1}$$

Here, we follow the scheme of ref 19. Using the thermodynamic potential of Fredrickson and Helfand,[18] the Landau free energy density is written as a function of the amplitude A of the composition pattern:[19]

$$f(A) = \rho_c k_B T \left(\tau_R A^2 + \frac{u_R}{4} A^4 + \frac{w_R}{36} A^6 \right) \tag{4.2}$$

where ρ_c is the number density of polymer chains and $k_B T$ is Boltzmann's constant times temperature. τ_R, u_R, and w_R are renormalized thermodynamic coefficients. They are functions of χN, the Flory–Huggins interaction parameter per monomer times the number, N, of monomers in a chain,[19,20] and of a dimensionless degree of polymerization, $\bar{N} \equiv 6^3 (R_g^3 \rho_c)^2$, where R_g is the radius of gyration of a polymer chain. Fredrickson and Binder[19] expressed these terms in rescaled, reduced form. We prefer to retain the dimensional and unreduced variables and

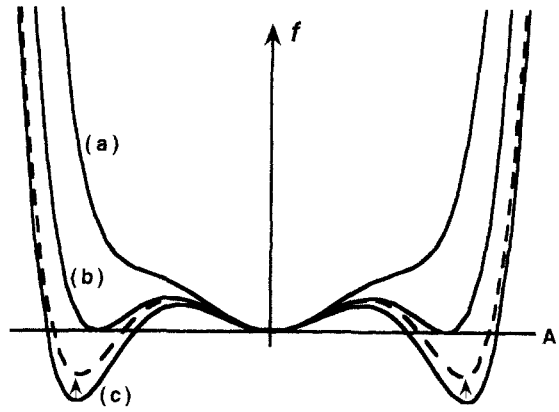

Figure 4. Landau free energy for (a) $T > T_{ODT}$, (b) $T = T_{ODT}$, and (c) $T < T_{ODT}$, as a function of the amplitude of a hypothetical composition pattern. When an electric field is applied, the free energy is augmented to give the dashed curve (in the case of (c)). The increase in the free energy is a function of lamellar orientation with respect to the external field.

follow the notation of ref 21. (The terms of eq 4.2, therefore, have slightly different meanings in this work than in ref 19; see ref 21 for a comparison of term definitions.) The behavior of this polynomial and its ramifications for the phase behavior of a symmetric block copolymer have been explored by Fredrickson and Binder.[19] The polynomial is shown for various values of χN near the order–disorder transition (ODT) in Figure 4. The minimum at A equal to zero corresponds to the disordered phase, the minimum at finite A corresponds to the ordered phase.

In an electric field, the free energy is augmented by an electric term given to second order by eq 1.1. Adding this term to the Landau free energy density of eq 4.2 gives

$$f(A) = \rho_c k_B T\left[(\tau_R + \eta_{elec})A^2 + \frac{u_R}{4}A^4 + \frac{w_R}{36}A^6\right] \quad (4.3)$$

where

$$\eta_{elec} = \frac{1}{4\pi}\frac{\left[(\beta^2/\epsilon_D)(\hat{\mathbf{e}}_q\cdot\hat{\mathbf{e}}_z)^2 - \frac{1}{2}(\partial^2\epsilon/\partial\psi^2)\right]|\mathbf{E}_0|^2}{\rho_c k_B T} \quad (4.4)$$

η_{elec} is an electric field energy density times the volume of a polymer chain divided by thermal energy. In eq 4.3 an inconsequential term independent of the composition pattern amplitude, A, is dropped. Also, there are fourth-order and higher electrostatic contributions which are neglected because they are much smaller than the quadratic term. The first term in the brackets is anisotropic in the lamellar alignment direction and is non-negative. The second term reflects the desire of the copolymer segments to mix (for $\partial^2\epsilon/\partial\psi^2 > 0$) or demix (for $\partial^2\epsilon/\partial\psi^2 < 0$) in order to increase the space-average dielectric constant, and this term will shift the ODT very slightly. The effect of this term has recently been observed and studied for a polymer solution near the critical point.[22] However, since this term is isotropic and small, it will not contribute directly toward alignment and will be considered no further.

The effect of the electric energy on the free energy polynomial is illustrated in Figure 4. The minima corresponding to the ordered state are raised slightly by the electric field and by a different amount for different orientations (specifically, different $(\hat{\mathbf{e}}_q\cdot\hat{\mathbf{e}}_z)^2$). The result is that the order–disorder transition and upper metastability limit of the ordered phase will be shifted slightly in temperature by an amount dictated by η_{elec}.

At this point we note that the electric field contribution to the Landau free energy is equivalent in form to the contribution due to mechanical deformation of the lamellar pattern. The latter was recently considered.[21] On the basis of the similarity between the electrostatic energy and the energy of mechanical deformation, a result from ref 21 is used to arrive at the condition for the ODT in the presence of an applied field:

$$\chi_t N = \chi_s N + 37.823\bar{N}^{-1/3} + 0.79022\eta_{elec} \qquad \eta_{elec} \ll 1 \quad (4.5)$$

$\chi_t N$ is the value of χN at the ODT, and $\chi_s N$ is the value at the mean-field spinodal, which is 10.495 for a symmetric copolymer.[20] The second term on the right arises as a result of composition fluctuations,[18] and the third term is the orientation-dependent shift due to the applied field, where η_{elec} is given by eq 4.4. By insertion of eq 4.4 into eq 4.5, the difference in χN at the ODT between ordered phase regions with lamellae perpendicular ($(\hat{\mathbf{e}}_q\cdot\hat{\mathbf{e}}_z) = 1$) to those parallel ($(\hat{\mathbf{e}}_q\cdot\hat{\mathbf{e}}_z) = 0$) to the applied field is

$$\Delta\chi_t N \equiv \chi_t N|_\perp - \chi_t N|_\parallel = 0.062884\frac{(\beta^2/\epsilon_D)|\mathbf{E}_0|^2}{\rho_c k_B T} \sim 8 \times 10^{-5} \quad (4.6)$$

The material parameters $\epsilon_{PS} = 2.55$, $\epsilon_{PMMA} = 3.78$, $\beta = \epsilon_{PMMA} - \epsilon_{PS}$, $\epsilon_D = (\epsilon_{PS} + \epsilon_{PMMA})/2$, $\rho_c = 6.44 \times 10^{21}$ cm^{-3}, and $T_{ODT} = 251$ °C and the field strength of 60 statvolt/cm (=18 kV/cm) were used to arrive at the numerical value. From the temperature dependence[23] of χ one finds that this corresponds to a difference in ODT temperatures of

$$\Delta T_{ODT} \equiv T_{ODT,\perp} - T_{ODT,\parallel} = -0.0037 \text{ K} \quad (4.7)$$

between the perpendicular and parallel lamellar orientations. Selective disordering of microstructure in a disfavored orientation while maintaining lamellae in preferred orientations could occur only if the sample were within a few millikelvin of its zero-field ODT. Since the microstructure was aligned several degrees below the ODT, alignment was achieved by another mechanism. A more likely pathway for the alignment process will be considered next.

Before moving on, it is worth noting that the difference in ODT temperatures for the parallel and perpendicular alignment scales quadratically with field strength. In an applied field on the order of 5×10^5 V/cm, near the dielectric breakdown limit for many polymers, the difference in ODT temperatures will be approximately 3 K, an experimentally accessible value. Also, it should be noted that *mechanical* deformations can induce a much greater ODT temperature shift than an electric field, since there is no mechanical analogue to the dielectric breakdown strength of the polymer.[21] In fact, deformation-induced disordering has been proposed as an alignment mechanism.[7,8]

B. Alignment by Defect Movement. The texture of the aligned block copolymer sample suggests that alignment occurs by movement and annihilation of defect structures. This mechanism is considered here. First, the texture of the microstructural pattern is considered; then forces on defect structures are examined.

1. Textures and Defect Structures. The rotational and translational symmetries of the lamellar block copolymer microstructure are the same as for the smectic-A liquid crystal phase. For this reason, fundamental similarities in textures are expected. Type $\pm^1/_2$ disclination lines and wall defects, prevalent in lamellar block copolymer samples (cf. Figure 3), are also seen in smectic-A

systems.[13-17,24] Despite the similarities, there are differences in the large-scale texture of the microstructure in the block copolymer sample reported on here and common smectic-A textures.

Smectic-A textures typically involve splay of the lamellar normal and very little layer compression or dilation. They contain positive half-integer and integer disclination lines. These defects themselves do not introduce layer dilation, but to fill three-dimensional space some dilation is present at any of four related features: focal lines, walls, $-1/2$ disclination lines, or dislocations.[14,15] In addition, the dilation introduced by one of these may be relaxed by another of opposite sign. The morphology that we find in this study is consistent with the presence of $+1/2$ disclination lines and wall defects, and each of the four related features. However, $-1/2$ disclination lines and isolated edge dislocations are rare.

To understand the existence of $\pm 1/2$ disclination lines, recognize that a pair of disclination lines of opposite signs is topologically equivalent to a dislocation[13] (illustrated below). Kleman[13] has calculated the energy of a compound dislocation (disclination line pair) having Burgers vector magnitude b:

$$W = \frac{K_1|b|}{\lambda} + \frac{\pi K_1}{2}\ln[b/(2d_0)] + W_{\text{core}} \qquad (4.8)$$

where K_1 is the splay elastic constant of the lamellar microstructure,[21,25] W_{core} is the energy of the disclination line or dislocation core, and d_0 is the equilibrium layer spacing. K_1 is the elastic splay constant of the lamellar composition pattern,[21] and λ is defined as

$$\lambda = (K_1/\bar{B})^{1/2} \qquad (4.9)$$

where $\bar{B}$ is the layer compressibility.[21] This leads to the following inequality:

$$W(b_1 + b_2) < W(b_1) + W(b_2) \quad \text{for} \quad b_1, b_2 > 2d_0 \qquad (4.10)$$

indicating that defects are more stable when clustered. For this reason, elementary dislocations are rare and disclination line pairs are more frequent.[16]

Despite the formal similarities, the texture of block copolymer microstructure is quite distinct from the texture commonly seen in smectic-A materials. A smectic-A material not aligned by surfaces or body forces typically exhibits the focal conic structure where the defects are arranged in such a manner as to permit continuity of layering.[13,17,24] In the case of block copolymers, the texture is not so organized as to give the focal conic texture. Perhaps the main reason is the relatively high viscosity of polymeric systems, and the associated slow approach to low-energy states. Also, the driving force toward the focal conic texture should depend upon the energies of defect walls and core energies of disclination lines and edge dislocations. These quantities may differ greatly between the block copolymer and the smectic systems. Differences in the natural length scale, the penetration depth[13,17,24,26] λ, could also account for differences in texture. (However, calculations suggest that the penetration depth of block copolymers is similar to that of smectic-A materials.[21])

2. Alignment Proceeding through Disclination Line Motion and Annihilation. Without an aligning field, the disclination lines are expected to be isotropically distributed. After application of a field, our results show an anisotropic distribution of disclination line orientations, with disclination lines predominantly along the field direction. There are at least two ways this could have come to be. One is that, through action of the field, disclination lines that are originally not aligned with the field are caused to rotate to be aligned with the field. However, such a movement is rather formidable. It would involve very long-range motion of disclination lines and associated large-scale re-formation of the lamellar pattern. We consider a more reasonable explanation to be that alignment is accomplished through disclination line motion leading to annihilation of those transverse to the field. Defect walls in the aligned sample also have an anisotropic arrangement, indicating that under the influence of an electric-field defect walls move and annihilate as well. For completeness, it should be mentioned that alignment can also be achieved by nucleation and growth of defect structures, such as a focal conic $+1/2$ disclination loop and an associated focal line.[13]

Next, in support of the above hypothesis, we calculate forces on defect structures in an electric field. A full treatment of the problem is difficult because it involves interactions between many defects. It is instructive to consider instead some simple cases: a general wall defect, a $+1/2$, $-1/2$ pair of parallel disclination lines, and two compound edge dislocations with opposing Burgers vectors.

3. Electric-Field-Induced Forces on Wall Defects. Electric-field-induced forces on defect walls are particularly easy to calculate because the distortion to the lamellar pattern is limited to a small (molecular scale) region within the proximity of the wall. Examples of wall defects can be seen in Figure 3a. In the absence of an electric field the free energy densities of the material on the two sides of a wall are equal. This degeneracy is lifted in an electric field because of the different alignments of the lamellae on each side with respect to the field. This free energy difference produces a normal stress on the defect wall, $\underset{\approx}{\sigma}_{\text{elec}}$, proportional to the free energy density difference

$$\underset{\approx}{\sigma}_{\text{elec}} = \frac{1}{8\pi}\mathbf{E}_0^2\frac{\beta^2}{\epsilon_D}\langle\bar{\psi}^2\rangle[(\hat{\mathbf{e}}_{q,1}\cdot\hat{\mathbf{e}}_z)^2 - (\hat{\mathbf{e}}_{q,2}\cdot\hat{\mathbf{e}}_z)^2]\hat{\mathbf{n}}\hat{\mathbf{n}} \qquad (4.11)$$

where $\hat{\mathbf{e}}_{q,1}$ and $\hat{\mathbf{e}}_{q,2}$ are the unit vectors in the direction of the lamellar pattern wave vectors on the two sides of the wall and $\hat{\mathbf{n}}$ is a unit vector normal to the wall. The stress drives the wall to move toward the side for which $(\hat{\mathbf{e}}_q\cdot\hat{\mathbf{e}}_z)^2$ is largest.

The only walls that do not experience a field-induced force are those for which on both sides the alignment of lamellae with respect to the electric field is equally good (*i.e.* $(\hat{\mathbf{e}}_{q,1}\cdot\hat{\mathbf{e}}_z)^2 = (\hat{\mathbf{e}}_{q,2}\cdot\hat{\mathbf{e}}_z)^2$). In fact, these are precisely the wall defects which are most prevalent in the field-aligned sample.

4. Forces on Disclination Lines. a. General Principles. Disclination lines have associated with them an extended distortion field. The total free energy of disclination lines includes an integral over the free energy density associated with the distortion. To lowest order, the free energy density is[21]

$$f = \frac{1}{2}\bar{B}\gamma^2 + \frac{1}{2}K_1(\nabla\cdot\hat{\mathbf{e}}_q)^2 + \frac{1}{8\pi}\frac{\beta^2}{\epsilon_D}\langle\bar{\psi}^2\rangle(\hat{\mathbf{e}}_q\cdot\mathbf{E}_0)^2 \qquad (4.12)$$

The first term expresses the energy density associated with compression or expansion of the layers. γ is the compression or expansion layer strain and $\bar{B}$ is the layer compressibility (not to be confused with bulk compressibility). The second term represents the energy associated with a splay distortion (the molecules undergo splay, the layer planes bend), and K_1 is the splay electric coefficient.

The third term is the second-order anisotropic electrostatic energy from eq 1.1.

From this expression two important length scales arise. One is analogous to the so-called "penetration depth",[13,24] λ, of the smectic-A liquid crystal phase and was defined in eq 4.9. This length scale is important in controlling the shape of the distortion pattern around defect lines and the length scale of certain instabilities, for example. λ is typically on the order of or somewhat smaller than the layer spacing for liquid crystal systems. For block copolymers, λ has been calculated to be about one-quarter of the molecular size, about 1 order of magnitude smaller than the lamellar period.[21,25]

In the presence of an electric field, an electric length scale can be defined:

$$\xi = \left(\frac{4\pi K_1}{\frac{\beta^2}{\epsilon_D}\langle \bar{\psi}^2 \rangle E^2} \right)^{1/2} \tag{4.13}$$

where E^2 is a square electric-field strength relevant to the problem. This term is analogous to a length scale defined for nematics in magnetic fields.[24,27] Using the calculated value for K_1 of $1.8213\rho_c k_B T R_g^2 \langle \bar{\psi}^2 \rangle$ from ref 21, the electric length scale can be rewritten as

$$\xi = \left[\frac{22.89\rho_c k_B T R_g^2}{(\beta^2/\epsilon_D)E^2} \right]^{1/2} \tag{4.14}$$

For the block copolymer sample in this study, ρ_c is 2.0×10^{19} cm^{-3}, R_g is 5.8 nm, β is approximately 1.2, and ϵ_D is approximately 3.2. The field strength is 18 kV/cm (60 statvolts/cm in Gaussian units) and the alignment temperature was near 520 K. These numbers give an electric length scale of order 500 nm, which is about 23 lamellar periods.

The significance of the electric length scale is that distortion wavemodes with wavelengths less than ξ are dominated by mechanical terms, while those with wavelengths greater than ξ are dominated by the electrostatic energy.

b. Forces on Paired Disclination Lines. We begin by considering a pair of straight, parallel disclination lines of strengths $+1/2$ and $-1/2$ in an otherwise homogeneous block copolymer sample, as shown in Figure 5a. (Pairs of disclination lines can be seen in Figure 3c. Also, some very clear disclination line pairs were observed by Dlugosz and co-workers[28] in an extruded polystyrene–polybutadiene block copolymer.) There is a core energy associated with the distortion within one-half layer spacing of the disclination lines[13] and an energy associated with the distortion field outside the core. The latter adds to both the mechanical and electrical energies of the material.

The distortion field can be divided into two components:[13] the lamellae forming approximately semicircular arcs within a semicylindrical region between the disclinations (shaded region of Figure 5a), and a weak but extensive distortion emanating in the x_3 direction from the disclinations. The far-field distortion is primarily within the two parabolic regions defined by[13,26]

$$x_1^2 < 4\lambda|x_3| \tag{4.15}$$

above and below the disclination line pair.

It is important to realize that the far-field distortion cannot be eliminated even when the two disclination lines are brought together. The disclination lines can meet only by performing the layers between them, and thus leaving behind a set of edge dislocations with a total Burgers vector

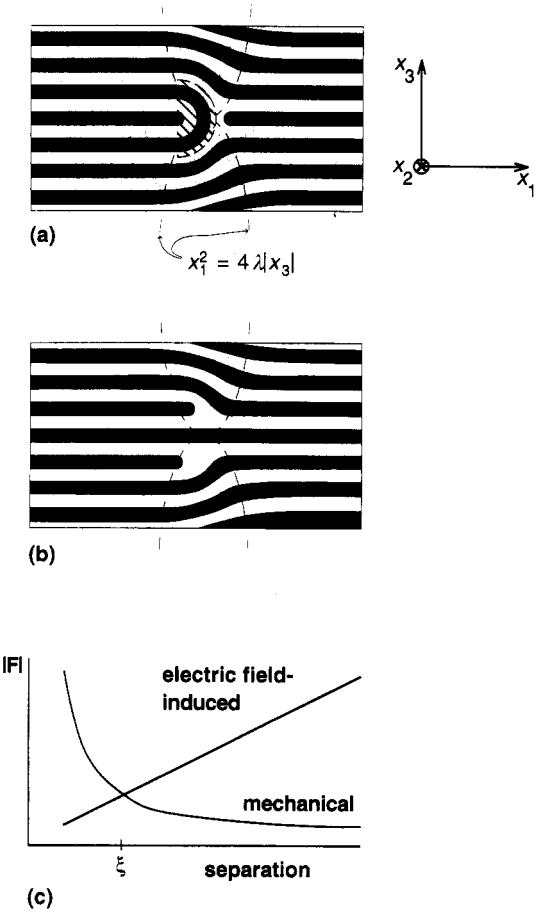

Figure 5. (a) Representation of a cross sectional cut through a block copolymer material that is well ordered except for a pair of straight, parallel $+1/2$ and $-1/2$ disclination lines normal to the page. For clarity, the composition pattern is represented as black and white stripes. The semicylindrical region of "near field" distortion is crosshatched. A local coordinate system (x_1, x_2, x_3) is defined by the interline vector (along x_1) and the asymptotic lamellar normal (x_3), as shown. In (b), the hypothetical situation where the two disclination lines have met and annihilated is shown. In this specific case, a layer is perforated to achieve the meeting of the lines, leaving behind two incomplete layers. Note that the net Burgers vector is unchanged, and the far-field distortion pattern is similar to that in (a). (c) shows a schematic of the magnitude of the mechanical and electric-field-induced forces along x_3 due to lamellar distortion.

which would equal the original Burgers vector of the pair of disclination lines (see Figure 5b). The far-field distortion pattern, which is tied to the net Burgers vector, will not change. However, the near-field pattern can be eliminated by movement of the disclination lines toward one another. Thus, in calculating the energy of attraction between the line pair, only the energy associated with the near-field pattern is considered. One ought to include, however, the energy penalty associated with creating edge dislocations when the lines move together, but this quantity is unknown.

Within the semicylindrical region the primary distortion is splay and the layer planes are approximately semicircular. The radius of curvature of the splay equals the distance from the $+1/2$ disclination line. Integrating the free energy density of eq 4.12 over the semicylindrical region gives the free energy of distortion including an electrostatic contribution:

$$W = \frac{1}{2}K_1 L \ln\left(\frac{b/2}{r_{core}}\right) + \frac{1}{128}\frac{\beta^2}{\epsilon_D}\langle \bar{\psi}^2 \rangle b^2 L(E_1^2 - E_3^2) \tag{4.16}$$

where r_{core} is the lower radial limit of integration about

the $+^1/_2$ disclination line and is the radius of the disclination line core (of order one lamellar spacing) and L is the length of the disclination line. b is the magnitude of the Burgers vector of the disclination line pair, equal to twice the distance between the lines, minus two lamellar periods. E_1 and E_3 are components of the electric field in the local x_1 and x_3 directions, respectively (see Figure 5a). The forces between the disclinations as predicted by this equation are shown in Figure 5c. The field-induced force is attractive if the pattern is aligned with the field far from the disclinations ($E_1 > E_3$) or repulsive if the pattern is aligned contrary to the preferred direction ($E_3 > E_1$). For small separations the force due to mechanical distortion is dominant, while for large separations the electrical force is greater. The crossover distance at which the two are equal is at the Burgers vector

$$b_0 = \left(\frac{32K_1}{\frac{\beta^2}{\epsilon_D}\langle\bar{\psi}^2\rangle|E_1^2 - E_3^2|} \right)^{1/2} \qquad (4.17)$$

which for the experiment of this report is on the order of 0.5 μm (for the case where the field is along x_1).

The electric field induces a repulsive or attractive force between the pair of disclination lines, depending upon whether increased separation results in greater or lesser alignment with the electric field. For example, consider the case where the block copolymer sample is well-aligned by an electric field, except for a pair of parallel disclination lines of opposing sign running through the sample (as in Figure 5a where the field is along x_1). The lamellar pattern is reoriented away from lowest-energy orientations by the distortion pattern, and the electric field will induce an attractive force between the defects, thus coercing them to come together and annihilate. Conversely, disclination line pairs in regions where the lamellar pattern is predominantly aligned in a high-energy orientation, such as when the far-field lamellar wave vector is parallel to the applied field, will experience a repulsive field-induced force (consider Figure 5a with the field along x_3). The only pair of disclination lines which will not experience a field-induced force are the lines which run in the direction of the applied field (consider Figure 5a with the field along x_2). These are precisely the types of disclination lines prevalent in the field-aligned sample.

Also, as stated above, the field-induced force can only be important when the separation between the disclination lines exceeds the electric length scale, ξ, which is on the order of 0.5 μm. The electric field could therefore act to bring disclination lines to within a distance comparable to the electric length scale. Beyond that, normal mechanical forces would be responsible for closer approach and eventual annihilation. For cases where the field-induced forces push a pair of disclination lines apart, the force increases with separation. One can envision continued separation until the disclination lines are annihilated by coalescence into another defect, such as a defect wall.

c. Forces on Paired Compound Edge Dislocations. Next, we consider the interaction between a pair of oppositely-signed compound edge dislocations, as shown in Figure 6. Each compound edge dislocation is made up of a pair of oppositely-signed disclination lines, and in far field is similar to a simple edge dislocation but with a larger Burgers vector. (The magnitude of the Burgers vector is equal to twice the separation between the lines minus two lamellar periods.[13]) Since the sum of the Burgers vectors is zero, the far-field distortion disappears when the compound edge dislocations approach each other

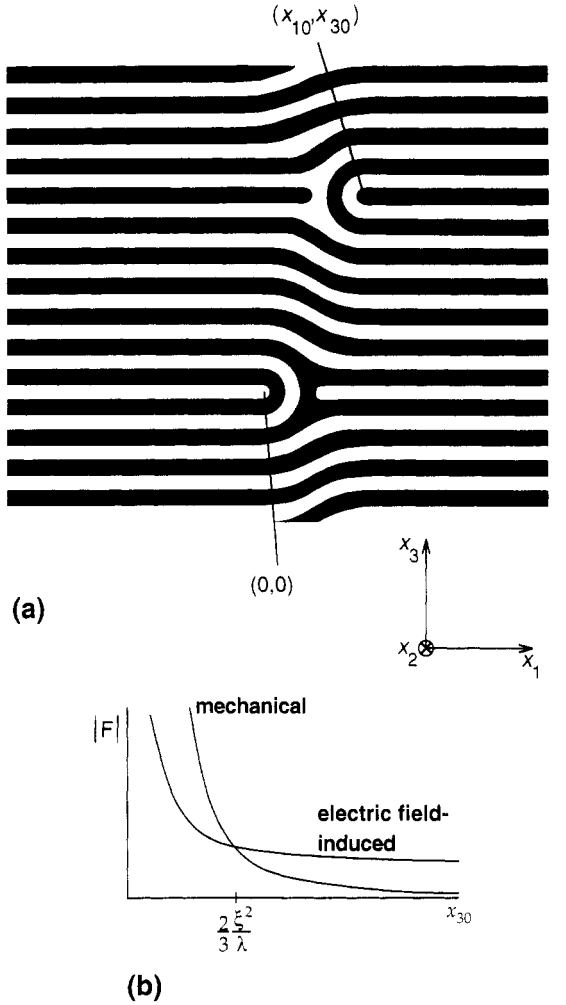

Figure 6. (a) Cross sectional cut through a block copolymer material which is well ordered except for two pairs of oppositely signed disclination lines. Each pair makes up a compound dislocation of Burgers vector equal to twice their separation minus two lamellar periods. In this illustration the Burgers vector has a length equal to two lamellar periods. The local coordinate system (x_1, x_2, x_3) is as defined in Figure 5, and the centers of the dislocations are indicated by (x_1, x_3) coordinates. In (b) the magnitude of the force between the two compound edge dislocations is shown for the case where they are vertically displaced. The contributions due to splay and compression of the microstructural pattern (denoted "mechanical") and due to the electric field are shown.

and annihilate. This behavior is quite distinct from the previous example where the sum of the Burgers vectors was non-zero.

This problem has been previously solved, for the case of zero electric field, by Kléman and Williams,[29] using an expression for the distortion field from a single edge dislocation developed by de Gennes.[26] Here, their method is repeated, but including the electric-field energy.

The energy of deformation in the field can be expressed in terms of the scalar strain field variable $u(\mathbf{r})$:

$$f = \frac{1}{2}\bar{B}\left(\frac{\partial u}{\partial x_3}\right)^2 + \frac{1}{2}K_1\left(\frac{\partial^2 u}{\partial x_1^2}\right)^2 + \frac{1}{8\pi}\frac{\beta^2}{\epsilon_D}\langle\bar{\psi}^2\rangle\left[(E_1^2 - E_3^2)\left(\frac{\partial u}{\partial x_1}\right)^2 - 2E_1E_3\frac{\partial u}{\partial x_1}\right] \qquad (4.18)$$

for small distortions. Here, $u(\mathbf{r})$ is the change in elevation of the layers with respect to the case where the layers are undistorted and horizontal.[12,21] This equation was obtained by re-expressing the three energy densities of eq 4.12 in terms of the strain variable u for small distortions.

The equation of equilibrium, derived from eq 4.18 by a variational principle, is

$$\bar{B}\frac{\partial^2 u}{\partial x_3^{\,2}} - K_1\frac{\partial^4 u}{\partial x_1^{\,4}} + \frac{1}{4\pi}\frac{\beta^2}{\epsilon_D}\langle\bar{\psi}^2\rangle(E_1^{\,2} - E_3^{\,2})\frac{\partial^2 u}{\partial x_1^{\,2}} = 0 \tag{4.19}$$

The edge dislocation with Burgers vector of length $+b$ along x_3 is at (0,0) and the one with Burgers vector $-b$ is at (x_{10},x_{30}). Because the equation of equilibrium is linear, the distortion pattern is simply the sum of the distortion patterns of the dislocations taken separately. Following the method of deGennes[26] and Kléman[13,16] while including the new electric energy term of eqs 4.12, 4.18, and 4.19 yields displacement field as

$$u(x_1,x_3) = \begin{cases} f_+(x_1,x_3) + f_+(x_1 - x_{10}, x_3 - x_{30}) & x_3 > x_{30} \\ f_+(x_1,x_3) + f_-(x_1 - x_{10}, x_3 - x_{30}) & 0 < x_3 < x_{30} \\ f_-(x_1,x_3) + f_-(x_1 - x_{10}, x_3 - x_{30}) & x_3 < 0 \end{cases} \tag{4.20}$$

where

$$f_\pm(v,w) = \pm\frac{b}{4} \pm \frac{b}{4\pi}\int_{-\infty}^{\infty} dq\, \frac{e^{iqv}}{iq} \exp\left[\mp\lambda q^2\left[1 + \frac{1}{(\xi q)^2}\right]^{1/2} w\right] \tag{4.21}$$

and (cf. eqs 4.13 and 4.14)

$$\xi = \left[\frac{4\pi K_1}{(\beta^2/\epsilon_D)\langle\bar{\psi}^2\rangle(E_1^{\,2} - E_3^{\,2})}\right]^{1/2} \tag{4.22}$$

is an electric length scale for this problem.

Equation 4.20 reduces to the equation of Kléman and Williams[29] in the absence of an electric field. The effect of the electric field is to reduce the amplitude of long-wavelength components of the distortion pattern (for which ξq is small or of order unity). These components are found at vertical distances

$$x_3 \geq \pi^2\frac{\xi^2}{\lambda} \tag{4.23}$$

from the dislocations.

In the case where the projection of the electric field along x_3 exceeds the projection along x_1 ($E_3 > E_1$), ξ is imaginary. In this case, small-q modes ($\xi q < 1$) are oscillatory and are inconsistent with the primary assumption of vanishing distortion at large distances. Physically, this corresponds to the ripple instability analogous to the Helfrich–Hurault instability seen in cholesteric and smectic liquid crystal materials which appear above a critical electric field (or dilatative mechanical stress) normal to the layer planes. The critical value decreases to zero as the extent of the sample along the x_3 direction increases to infinity. This regime, although interesting, will be considered no further. We focus on the condition where ξ is real and E_1 is greater than E_3.

The total energy of the disclination line pair is obtained by applying eq 4.20 to the energy density expression of eq 4.18, and integrating over all space (with lower and upper cutoffs). The integration is simplified by keeping terms to only second order in $1/(q\xi)$; this is justified since $1/(q\xi)$ is small for all q-values of importance. The result is

$$W = W_{mech} + W_{elec} \tag{4.24}$$

where

$$W_{mech} = -\frac{KLb^2}{4\pi\lambda}\left(\frac{\pi}{\lambda x_{30}}\right)^{1/2}\exp\left(-\frac{x_{10}^{\,2}}{4\lambda x_{30}}\right) \tag{4.25}$$

and

$$W_{elec} = -\frac{1}{\xi^2}\left[\frac{1}{2}x_{30}\lambda W_{mech} + \frac{\lambda}{2}\int_0^{x_{30}} dx'_{30}\, W_{mech}(x'_{30}) + \frac{\bar{B}Lb^2\lambda}{8\pi}\int_{q_0}^{q_c} dq\,\frac{\cos(qx_{10})}{q^2}\right] + O(E^4) \tag{4.26}$$

Components that are independent of position and represent self-energy of the defects are not shown in the above expressions.

The mechanical term is the result of Kléman and Williams,[13,29] but the electric-field term is new. For the sake of simplicity, consider the case where the two dislocations are vertically aligned, that is, $x_{10} = 0$. In that case, a simple analytical form for the two energies can be found:

$$W_{mech} = -\frac{KLb^2}{4\lambda(\pi\lambda x_{30})^{1/2}} \tag{4.27}$$

and

$$W_{elec} = \frac{3}{8}\frac{KLb^2}{\xi^2}\left(\frac{x_{30}}{\pi\lambda}\right)^{1/2} + O(E^4) \tag{4.28}$$

ignoring terms with no position dependence. The mutual force of attraction between the dislocations has a mechanical contribution, F_{mech}, and an electric field contribution, F_{elec}:

$$F_{mech} = \frac{KLb^2}{8\pi^{1/2}(\lambda x_{30})^{3/2}} \tag{4.29}$$

and

$$F_{elec} = \frac{3KLb^2}{16\xi^2(\pi\lambda x_{30})^{1/2}} + O(E^4) \tag{4.30}$$

The two forces are plotted in Figure 6b as a function of disclination separation distance. The force due to mechanical distortion of the matrix is dominant at short distances, while the electric-field-induced force is longer range. The crossover occurs at the separation distance

$$x_{30} = \frac{2}{3}\frac{\xi^2}{\lambda} \tag{4.31}$$

For the material and field strength of this work, ξ is on the order of 500 nm (see section II) and λ is approximately 1.9 nm. Therefore, the crossover length is on the order of 100 μm. This value is far greater than the distance over which defect-induced screening occurs.

From the determination of forces on defect structures the following conclusions can be drawn. Electric-field induced forces on wall defects can cause them to propagate and even annihilate upon meeting other wall defects. For line defects, the electric-field-induced forces are dominant only when the distance between lines (or radius of a disclination line loop) is greater than ξ. Thus, the electric field may induce movement of line defects in ways that improve alignment. Once the interdefect separation is less than ξ, mechanical forces dominate and accelerate the annihilation. Finally, it is unlikely that the electric field causes movement of compound edge dislocations, as the mechanical forces are stronger.

C. Defect Mobility. 1. Defects Moving through the Action of Dislocations (Climb or Glide). So far, electric-field-induced forces on defect structures have been determined. In order to understand the rate of alignment, defect *mobility* must now be addressed. First, the fundamental process by which defects move is considered. Next, the effect of defect interactions on mobility is considered.

Disclination lines (whether in textures of both positive and negative half-integer disclination lines or positive disclination lines with focal lines) are separated by a number of lamellae, so that lamellae must be removed as the lines approach one another and annihilate. This process may be accomplished through the motion of dislocation loops (both "climb" which is motion in the layer direction and "glide" which is motion transverse to the layers). In Figure 7a,b, a pair of disclination lines move closer together through perforation of a layer. In the case of layer perforation, the intermediate state is probably one in which the regions of perforation have a very small deviation from the average concentration. (Detailed activation energies have not been calculated yet.) Recall that near the ODT large fluctuations are present[18] so that nucleation of a perforation should not be uncommon. A dislocation loop marks the edge of the perforation. The loop widens by climb motion of the loop, and the edge dislocation at the core of the $+^1/_2$ disclination line climbs toward the $-^1/_2$ disclination line. In Figure 7c,d, a related process involving a focal conic structure is shown in cross section. Here, a vertical electric field induces a stress which encourages the formation of an island somewhere within the $+^1/_2$ dislocation loop. By growth of the island, the loop radius increases and the overall alignment of the material increases. In Figure 7e,f a mechanism by which a bend wall moves is shown. Here, an edge dislocation propagates along the wall through both climb and glide motion, resulting in translation of the wall.

Through the fundamental process of edge dislocation creation and movement, one can see how both line and wall defect structures move. These processes can be accomplished by sequential re-formation of the lamellar pattern on molecular scale, as suggested by Figure 7g,h. For this reason, one expects the temperature dependence of the rate of alignment to be determined by the temperature dependence of single chain motion. The latter was determined in a series of rheological experiments and expressed as a temperature shift factor.[10] Indeed, the rate of alignment at various temperatures was superimposed using the rheologically-determined temperature shift factor.[10]

2. Defect Interactions. a. General Principle. Defect interactions can strongly affect defect mobility. It is likely that these interactions are responsible for the clumping of defects observed in the aligned block copolymer sample.

There are two types of interactions; one is caused by direct contact as in the case of two wall defects in contact. The other is indirect interactions due to the distortion field emanating from disclination lines.

b. Interactions between Wall Defects and Other Defects. Wall defects may share common borders with other wall defects, as illustrated in Figure 8a. When an electric field is applied, the various walls experience forces in different directions. For instance, the center wall defect experiences a force toward the right. Movement of the wall defects involves a change in the total wall surface area which changes the surface energy of the set of walls. For this reason, the wall defects lose the translation invariance they have as isolated entities.

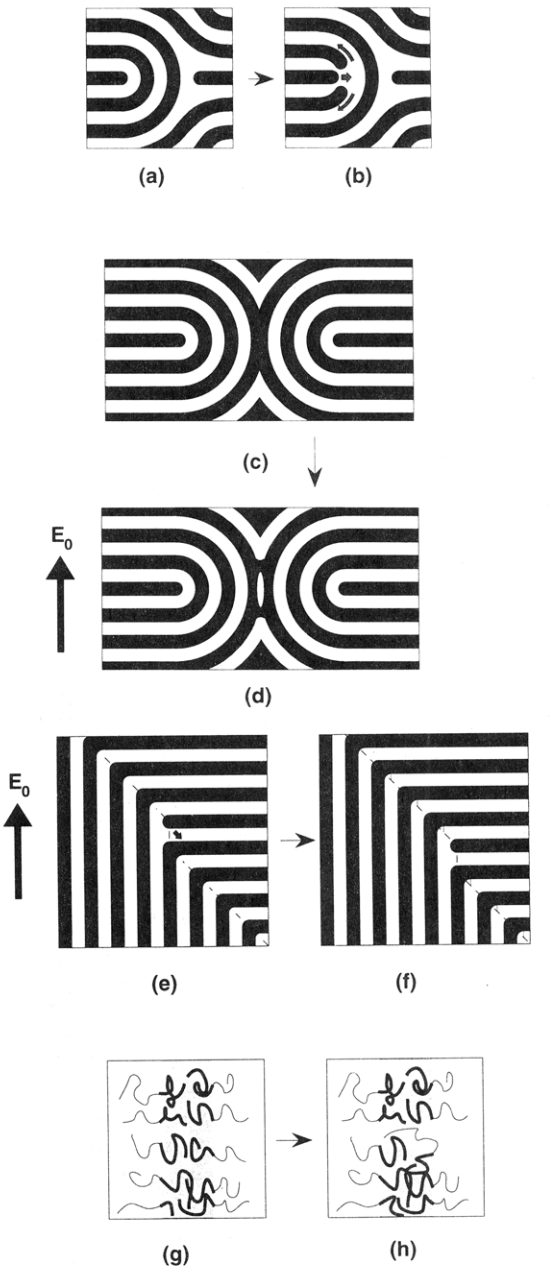

Figure 7. Movement of the disclination line and wall defects occurring by climb and glide of edge dislocations and creation of pores (edge dislocation loops). In (a), $+^1/_2$ and $-^1/_2$ disclination lines move closer through (b) perforation of a layer. Through "climb" motion (indicated by the curved arrows) the perforation opens up, and the edge dislocation at the core of the $+^1/_2$ disclination line "climbs" toward to the right. In (c) a focal conic loop is shown in cross section. It opens up (perhaps in response to a vertical electric field) through creation of an island in (d), which grows by climb motion of the associated disclination loop at the boundary of the island. In (e), a bend wall defect is shown in cross section. Through a combination of glide and climb motion, an edge dislocation propagates along the wall. After successive operations the wall translates one lamellar spacing to the right and up. In (g) a molecular scale representation of the lamellar pattern is shown, with light and dark lines representing the two components of a block copolymer. In (h) a pore is nucleated by molecular scale reorientation.

Another case involving direct contact of defects is shown in Figure 8b. Note that disclination lines must either form complete loops or end at the edge of the sample or, more likely, at a wall defect. For the defect wall to translate, in order to improve the overall alignment, the total length

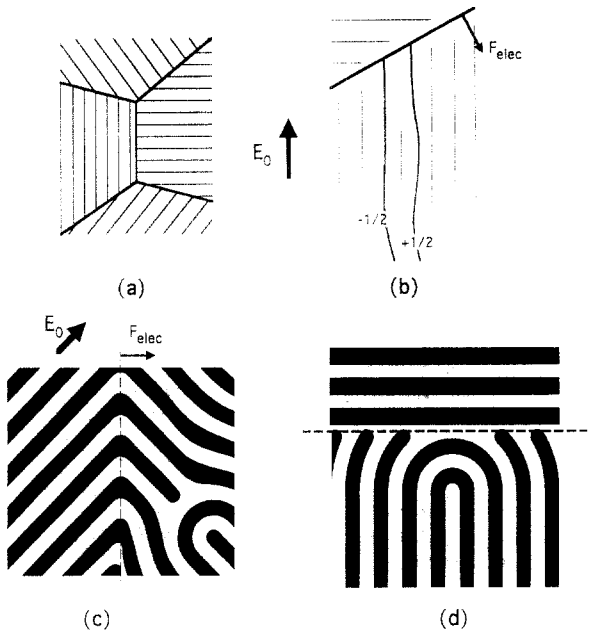

Figure 8. Situations where defects interact. Cases of interaction through direct contact are shown in (a) and (b) where wall defects are in direct contact with other wall defects or line defects, respectively. Cases of indirect interaction are shown in (c) and (d). Here, the distortion field emanating from line defects results in a mutual energy with a wall defect.

of line defects may need to be changed. For this reason also, the wall defect energy loses translation invariance.

Wall defects may also interact with distortions in the lamellar pattern. A simple example involves a "perpendicular bisector" wall, such as shown in Figure 8c. The perpendicular bisector wall is at an equal angle from the lamellar pattern on both sides of the wall. Many of this type of wall can be observed in block copolymer samples. The coherence of the lamellar pattern across the wall makes this a particularly favorable (low-energy) wall defect. As a bisector wall defect approaches a region of distortion, the coherence of the lamellar pattern is lost because the wall is no longer a perpendicular bisector of the lamellar pattern. Alternatively, the wall could distort in order to maintain the perpendicular bisector condition, resulting in an increase in the wall area. Either way the energy of the wall defect is increased.

For any of the several reasons mentioned above, defect interactions cause wall defects to lose translation invariance and, on average, reduce their effective mobility (see Figure 9a). If defect interactions create energy barriers larger than can be overcome by the electric-field force, they can pin defects and inhibit the aligning process (Figure 9b). For the case where forces due to defect interactions are small compared to the field-induced forces, the effect of defect interactions on the effective mobility can be understood in a simple way. Consider a single wall defect moving in an environment containing other defects. The velocity of the defect is equal to the sum of the forces imposed upon it divided by its intrinsic mobility μ:

$$v(x) = \frac{F_{elec} + F_{defect}(x)}{\mu} \tag{4.32}$$

For simplicity, we consider just forces and movement in one direction parameterized by x. F_{elec} is the field-induced force on the wall, and F_{defect} is the sum of forces from defect interactions and is a function of position. The average velocity of the defect in traversing a span L can

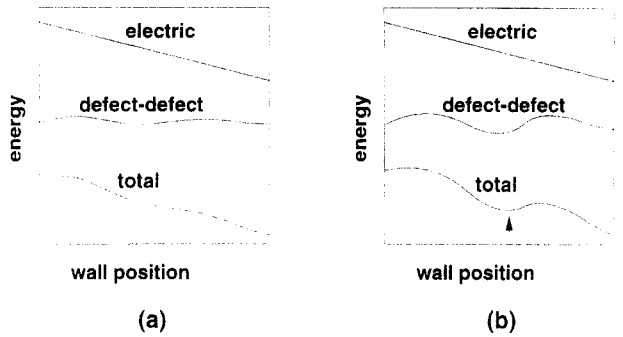

Figure 9. Schematic representation of the energy of a block copolymer material in an electric field as a function of the (linear) position of a wall defect. In the absence of defect interactions, the energy is a linear function of wall position (top curve), and the wall would drift smoothly in response to the electric field. Defect interactions contribute to the total energy (middle curves). In (a) the total energy (sum of electric energy and contributions from defect interactions) is monotonic. The wall defect will still migrate but with a reduced effective mobility. In (b), the energy has a local minimum at the position indicated by the arrow. If the energy barrier to escape is much more than thermal energy, the defect can be pinned at that position.

be expressed as

$$\langle v \rangle = L\left(\int_0^L \frac{dx}{v(x)}\right)^{-1} \tag{4.33}$$

In the case where F_{defect} is always much smaller than F_{elec} and the average of the defect forces is zero over the path of consideration, eq 4.33 gives to lowest order

$$\langle v \rangle \simeq v_0\left(1 - \frac{\langle F_d^2 \rangle}{F_{elec}^2}\right) \tag{4.34}$$

where v_0 is the velocity in the absence of defect interactions and $\langle F_d^2 \rangle$ is the space average square of the defect forces. The defect interactions have the effect, on average, of reducing the apparent defect mobility by a factor of $[1 - (\langle F_d^2 \rangle / F_{elec}^2)]$.

Figure 9b shows an example where the defect interaction forces have become larger than the electric-field force, and a local minimum in the defect energy exists at one or more positions. If the activation barrier to escape from one of these minima is much greater than the thermal energy, the defect can become pinned. An important point is that the effects of defect interactions become stronger with increasing defect density, not only because of the increased number of defect interactions but also because of the reduced size of the average wall defect (and thus reduced electric-field-induced driving force).

c. Interactions between Line Defects. Line defects interact with one another through their distortion fields, as shown in section IV.B.4. Line defects can also interact with wall defects in the manner shown in Figure 8d. Here, depending upon how the wall energy changes with the angle of the lamellae just below the wall, the wall defect will either be attracted to the wall or repelled from the wall. Line defects in the form of focal conics, or complete loops, are *self*-interacting. For all of these situations, the behavior of the forces on the defects as a function of the distance between defects (or radius of a loop defect) has the character shown in Figure 5c. When the separation between defects (or radius of disclination loop) is large, electric-field forces, which tend to rise linearly in the separation, dominate over mechanical forces. Mechanical forces decrease with this length scale (often with an inverse relationship) but become dominant at short distances. The crossover point is $O(\xi)$.

Just as with wall defects, when the density of defects increases, the length scale between them decreases, and the defect interactions become more important. The mobility of the line defects decreases accordingly, and for sufficiently high defect density, disclination lines may be pinned.

V. Manifestations of Defect Interactions

The interplay between electric-field-induced forces and defect interactions can explain several observable phenomena. For example, the rate of alignment was found to be much slower in a block copolymer that was cooled quickly from the disordered phase than for a sample that was cooled slowly.[10] The rapidly cooled sample had a much higher density of defects, and the higher defect density resulted in a lower effective defect mobility (as shown in the previous section). Also, the clumping of defects in the aligned sample discussed in section III is presumably due to an interplay between electric-field-induced and defect forces. Consider, for instance, a defect that migrates in response to an electric-field-induced force. As it enters a region of higher defect density, its likelihood of becoming pinned is increased. The result will be that defects will become clumped during the alignment process. It is noteworthy that the regions of high defect density seen in "parallel" microtome slices (*cf.* Figure 3c) tend to have a width transverse to the applied field that is $O(\xi)$.

VI. Comparison to Alignment by Deformation and Flow

The ability to align block copolymer microstructure by shear and elongational flow has been known for over two decades.[1] Several mechanisms have been proposed for the alignment process,[5,6,8] including disordering of regions of the ordered state that are distorted by the shear flow, followed by reordering in a preferred alignment direction.[7,8] When the rate of shear or elongation is much less than the lifetime of composition fluctuations, flow-induced alignment may have strong similarities to electric-field alignment and it is quite possible that alignment due to flow proceeds through defect movement. Elongational flow or the elongational component of shear will change the local periodicity of the lamellae when the lamellar wave vector is not along the velocity gradient or neutral direction. In a previous publication,[21] it was shown how a deformation raises the free energy in a manner similar to the way the electric field raises the free energy of the microstructure in certain orientations. Just as with electric-field alignment, some regions will experience a higher free energy than others. There will be an associated force, causing the defect structures to move in directions that decrease the size of regions where lamellae experience compression, expansion, or splay, as sketched in Figure 10. An equation similar to eq 4.12 could be developed, but where the anisotropic term is due to flow, not an electric field. Also, there would be a natural length scale analogous to the electric length scale, ξ, but which contains parameters of deformation instead of electric-field-related parameters:[30]

$$\xi_{mech} = \frac{\lambda}{|\alpha|} \tag{6.1}$$

in the case where the distortion is compression. α is the layer compressional strain. This length scale may be much smaller than the electric length scale, ξ, since the free energy changes on the ordered state due to deformation can easily be made much larger than the electric-field energy. For example, ξ_{mech} is on the order of eight lamellae for a 1% compression. As a consequence, defects would be not as easily pinned during flow alignment, and the "clumping of defects" seen in the electric-field-aligned sample discussed in this paper may not be seen in flow-aligned samples. It is notable that very good alignment of lamellae can be achieved by flow.[6-8,31]

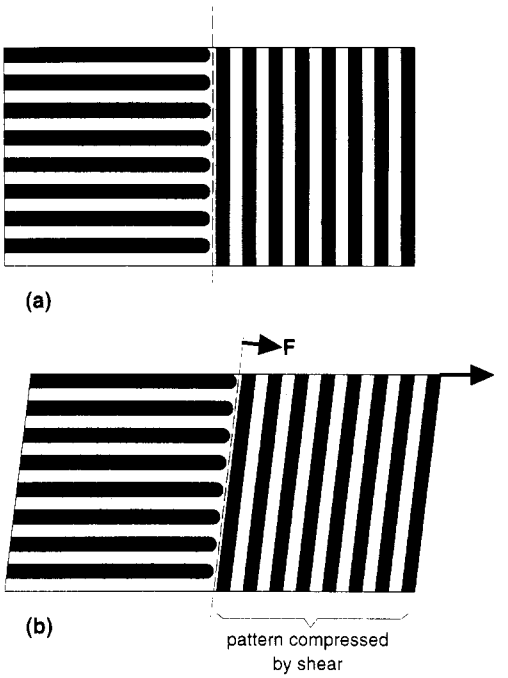

Figure 10. Simple illustration showing a block copolymer sample consisting of two regions of differing orientations separated by a wall defect. In (b) the sample undergoes a shear deformation. The pattern to the right of the wall is rotated and compressed. This raises its free energy, resulting in a force on the wall.

There are, however, important points of distinction between alignment by flow or deformation and alignment by an electric field. Flow involves bulk rotation of composition patterns, and electric fields do not. Also, when the rate of shear or elongation exceeds the lifetime of fluctuations, convection of composition fluctuations is expected to shift the transition temperature of the ordered phase, as predicted by Cates and Milner.[32] Koppi et al.[8] also point to the role of vorticity in shear flow alignment. Dynamic phenomena such as these have no analogy in the physics of electric-field alignment.

VII. Conclusions

In an electric field, lamellar block copolymer microstructure has an orientation-dependent free energy. For the material and field strength studied here, the size of the anisotropic component to the free energy is quite small. Notably, the electric-field energy over the volume of a polymer chain is far smaller than the thermal energy. Therefore, alignment of the microstructure must involve cooperative phenomena and large-scale structures. Electron micrographs of an aligned block copolymer sample give convincing evidence that alignment is achieved by movement and annihilation of disclination lines and defect walls. Calculations of both electric-field-induced forces on defect structures and defect interactions were considered. From consideration of the calculations, the scenario offered is one where defects move in response to field-induced forces in a manner which improves the overall alignment of the microstructure. Where disclination lines are involved, once the separation between defects drops below an electric length scale, ξ, field-induced forces are dwarfed by the usual mechanical forces, and the defect structures evolve as they would during annealing in the absence of an electric field. Through the interplay between defect interactions and field-induced forces, some under-

standing of the alignment kinetics and clumping of defects can be obtained.

Acknowledgment. We thank Frank Padden and Paul Szajowski for help with electron microscopy and Don D. Davis for small angle X-ray scattering work.

References and Notes

(1) Keller, A.; Pedemonte, E.; Willmouth, F. M. *Kolloid-Z. Z. Polym.* **1970**, *238*, 385.
(2) Folkes, M. J.; Keller, A. *Polymer* **1971**, *12*, 222.
(3) Hadziioannou, G.; Mathis, A.; Skoulios, A. *Colloid Polym. Sci.* **1979**, *257*, 136.
(4) Keller, A.; Odell, J. A. In *Processing Structure and Properties of Block Copolymers*; Folkes, M. J., Ed.; Applied Science: New York, 1985; p 29.
(5) Morrison, F.; Bourvellec, G. L.; Winter, H. H. *J. Appl. Polym. Sci.* **1987**, *33*, 1585.
(6) Morrison, F. A.; Winter, H. H. *Macromolecules* **1989**, *22*, 3533.
(7) Winey, K. I.; Patel, S. S.; Larson, R. G.; Watanabe, H. *Macromolecules* **1993**, *26*, 2542.
(8) Koppi, K. A.; Tirrell, M.; Bates, F. S.; Almdal, K.; Colby, R. H. Submitted for publication in *J. Phys. (Paris)*.
(9) Amundson, K.; Helfand, E.; Davis, D. D.; Quan, X.; Patel, S. S.; Smith, S. D. *Macromolecules* **1991**, *24*, 6546.
(10) Amundson, K.; Helfand, E.; Quan, X.; Smith, S. D. *Macromolecules* **1993**, *26*, 2698.
(11) Amundson, K.; Helfand, E.; Quan, X.; Patel, S. S.; Smith, S. D. *Macromolecules* **1992**, *25*, 1935.
(12) de Gennes, P. G.; Prost, J. *The Physics of Liquid Crystals*; Clarendon Press: Oxford, U.K., 1993.
(13) Kléman, M. *Points, Lines and Walls*; Wiley: New York, 1983.
(14) Bouligand, Y. *J. Phys. (Paris)* **1972**, *33*, 525.
(15) Bouligand, Y. *J. Phys. (Paris)* **1973**, *34*, 603.
(16) Kléman, M.; Williams, C. E.; Costello, M. J.; Gulik-Krzywicki, T. *Phil. Mag.* **1977**, *35*, 33.
(17) Chandrasekhar, S.; Ranganath, G. S. *Adv. Phys.* **1986**, *35*, 507.
(18) Fredrickson, G. H.; Helfand, E. *J. Chem. Phys.* **1987**, *87*, 697.
(19) Fredrickson, G. H.; Binder, K. *J. Chem. Phys.* **1989**, *91*, 7265.
(20) Leibler, L. *Macromolecules* **1980**, *13*, 1602.
(21) Amundson, K. R.; Helfand, E. *Macromolecules* **1993**, *26*, 1324.
(22) Wirtz, D.; Berend, K.; Fuller, G. G. *Macromolecules*, in press.
(23) Russell, T. P.; Rex, P.; Hjelm, J.; Seeger, P. A. *Macromolecules* **1990**, *23*, 890. The authors of this work interpreted their data using the mean-field theory of Leibler.[20] To be consistent with our work, we chose to interpret their data using the Fredrickson–Helfand theory. This gives $\chi = 0.012 + 17.1/T$, which is different than the χ reported in this reference.
(24) de Gennes, P. G. *The Physics of Liquid Crystals*; Clarendon Press: Oxford, U.K., 1974.
(25) Kawasaki, K.; Ohta, T. *Physica* **1986**, *139A*, 223.
(26) de Gennes, P. G. *J. Phys. (Paris) Suppl.* **1969**, *30*, C4.
(27) Hudson, S. D.; Thomas, E. L. *Phys. Rev. A* **1991**, *44*, 8128.
(28) Dlugosz, J.; Folkes, M. J.; Keller, A. *J. Polym. Sci., Polym. Phys. Ed.* **1973**, *11*, 929.
(29) Kléman, M.; Williams, C. E. *J. Phys.* **1974**, *35*, L49.
(30) The expression for ξ_{mech} used the expression for the elastic constants derived in ref 21.
(31) Albalak, R. J.; Thomas, E. L. *J. Polym. Sci., Part B: Polym. Phys.* **1993**, *31*, 37.
(32) Cates, M. E.; Milner, S. T. *Phys. Rev. Lett.* **1989**, *62*, 1856.